JACS
JOURNAL OF THE AMERICAN CHEMICAL SOCIETY
Article
pubs.acs.org/JACS

A Library of Selenourea Precursors to PbSe Nanocrystals with Size Distributions near the Homogeneous Limit

Michael P. Campos,[†] Mark P. Hendricks,[†] Alexander N. Beecher,[†] Willem Walravens,[‡,†] Robert A. Swain,[†] Gregory T. Cleveland,[†] Zeger Hens,[‡,∥] Matthew Y. Sfeir,*[,§] and Jonathan S. Owen*[,†]

[†]Department of Chemistry, Columbia University, New York, New York 10027, United States
[‡]Physics and Chemistry of Nanostructures Group (PCN), Ghent University, B-9000 Ghent, Belgium
[∥]Center of Nano and Biophotonics, Ghent University, B-9000 Ghent, Belgium
[§]Center for Functional Nanomaterials, Brookhaven National Laboratory, Upton, New York 11973, United States

Supporting Information

ABSTRACT: We report a tunable library of *N*,*N*,*N*′-trisubstituted selenourea precursors and their reaction with lead oleate at 60−150 °C to form carboxylate-terminated PbSe nanocrystals in quantitative yields. Single exponential conversion kinetics can be tailored over 4 orders of magnitude by adjusting the selenourea structure. The wide range of conversion reactivity allows the extent of nucleation ([nanocrystal] = 4.6−56.7 μM) and the size following complete precursor conversion (d = 1.7−6.6 nm) to be controlled. Narrow size distributions (σ = 0.5−2%) are obtained whose spectral line widths are dominated (73−83%) by the intrinsic single particle spectral broadening, as observed using spectral hole burning measurements. The intrinsic broadening decreases with increasing size (fwhm = 320−65 meV, d = 1.6−4.4 nm) that derives from exciton fine structure and exciton−phonon coupling rather than broadening caused by the size distribution.

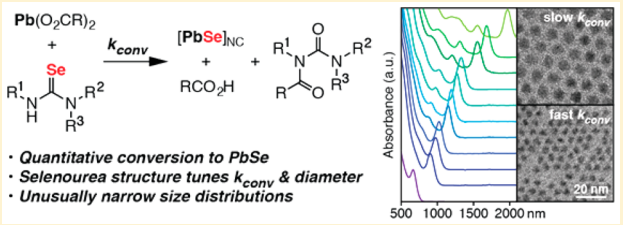

INTRODUCTION

Lead selenide (PbSe) nanocrystals have shown several highly desirable optoelectronic properties including efficient multiple exciton generation in photovoltaic devices[1−3] and the assembly of square and honeycomb lattices with topological states and Dirac cones in their band structure.[1−6] These lattices have potential to display unprecedented electrical transport behavior provided that disorder from the nanocrystal size distribution can be reduced.[7] However, it has proven challenging to synthesize PbSe nanocrystals from conventional nanocrystal precursors such as tri-*n*-alkylphosphine selenides, which are relatively unreactive toward lead carboxylate. Low yields of PbSe (<3%) are typically formed from more reactive secondary phosphine impurities in the tri-*n*-alkylphosphine starting material.[1−3,8,9] More recently, diphenylphosphine selenide,[1−6,9,10] *bis*(trimethylsilyl)selenide,[7,11] and other additives such as hexadecanediol[12] have been used to boost the conversion reactivity and improve the yield, but size control, and in particular, a high-yielding synthesis of PbSe nanocrystals relevant for photovoltaic cells (d < 3.9 nm, E_g > 1.0 eV), is needed.

In order to address the lack of selenium reagents with reactivity appropriate for the synthesis of PbSe, we developed a library of *N*,*N*,*N*′-trisubstituted selenoureas. The conversion reactivity of these precursors can be tailored by adjusting their substitution pattern, as we recently demonstrated using a library of analogous thioureas.[13] This tunable reactivity allows the rate of solute supply and the concentration of nanocrystals formed during nucleation to be adjusted[14−17] and the final size following complete precursor conversion to be controlled. Herein we report optimized precursors and conditions for the synthesis of PbSe nanocrystals across a broad range of sizes and at large scale. Narrow size distributions are obtained whose absorption spectral line widths are dominated by the intrinsic single-particle line broadening rather than heterogeneous broadening caused by the size distribution. These narrow distributions reveal a decreasing single particle spectral line width as the size of the nanocrystal increases.

RESULTS AND DISCUSSION

Di- and trisubstituted selenoureas can be synthesized from isoselenocyanates, LiAlSeH, NaHSe, $(Me_2Al)_2Se$, N-heterocyclic carbenes, carbon diselenide, and Woollins' Reagent ($[PhP(Se)(\mu\text{-}Se)]_2$),[18] but these approaches can be complicated because key reagents or intermediates are unstable or must be prepared in multiple steps. However, a few disubstituted selenoureas have been prepared in a single step from alkyl isocyanides, elemental selenium, and primary amines.[19−22] We have greatly expanded this approach to

Received: October 21, 2016
Published: January 19, 2017

DOI: 10.1021/jacs.6b11021
J. Am. Chem. Soc. 2017, 139, 2296−2305

Scheme 1. Synthesis of *N,N′*-Disubstituted and *N,N,N′*-Trisubstituted Selenoureas

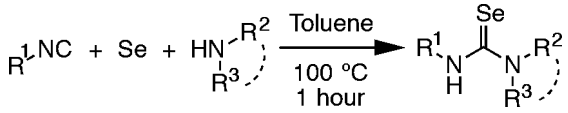

Table 1. Library of Selenoureas[a]

	R^1	R^2	R^3	yield (%)
1	*n*-C_4H_9	^{i}Pr	^{i}Pr	94
2[g]	*n*-C_4H_9	−$(CH_2)_5$−		95
3	*n*-C_4H_9	*n*-C_4H_9	*n*-C_4H_9	97
4	*n*-C_4H_9	Et	Et	94
5	*n*-C_4H_9	*n*-C_4H_9	Me	98
6	*n*-C_4H_9	Allyl	Allyl	97
7	*n*-C_4H_9	Me	Me	88
8[g]	*n*-C_4H_9	−$(CH_2)_4$−		68[b]
9	*n*-C_4H_9	4-MeO-Ph	Me	72[d]
10	Cy	*n*-$C_{12}H_{25}$	H	90[c]
11	Cy	Cy	Cy	65
12	Cy	^{i}Pr	^{i}Pr	57
13	Cy	^{i}Pr	Et	79
14	Cy	^{i}Pr	Me	90
15[g]	Cy	−$(CH_2)_5$−		82
16	Cy	*n*-C_4H_9	*n*-C_4H_9	76
17	Cy	Et	Et	84
18	Cy	Et	Me	69
19[g]	Cy	−2-Me-$(CH_2)_4$−		88
20[g]	Cy	tetrahydroisoquinolino		95
21	Cy	Allyl	Allyl	98
22	Cy	Me	Me	76[b]
23[g]	Cy	−$(CH_2)_4$−		89
24	Cy	4-MeO-Ph	Me	71
25	Cy	Ph	Me	64[e]
26	Cy	4-Cl-Ph	Me	27[f]
27	*n*-$C_{16}H_{33}$	^{i}Pr	Me	76
28	*n*-$C_{16}H_{33}$	Allyl	Allyl	63
29	*n*-$C_{16}H_{33}$	Ph	Me	73
30	^{t}Bu	Me	Me	72
31[g]	^{t}Bu	−$(CH_2)_4$−		68

[a]Reactions performed on 3 mmol scale for 1 h unless otherwise noted. [b]Performed on 6.6 mmol scale. [c]Performed on 10 mmol scale. [d]1.5 h reaction time. [e]2 h reaction time. [f]3 h reaction time. [g]Precursors with cyclic amino substituents (e.g. piperidino, pyrrolidino, 2-methylpyrrolidino, tetrahydroisoquinolino) as indicated by the dashed line in Scheme 1.

prepare a library of di- and trisubstituted selenoureas **1**−**31** in 60−98% yields (Scheme 1, Table 1). Unlike thioureas, tri- and disubstituted selenoureas are air-sensitive,[23] and in some cases slightly light-sensitive, eventually depositing elemental selenium over several months if stored under ambient conditions. Selenoureas are therefore best handled in the absence of air and stored in the dark, where they are indefinitely stable.

Isocyanides react with elemental selenium at 100 °C in toluene to produce isoselenocyanates that are trapped by a variety of nucleophilic amines to form di- and trisubstituted selenoureas. Formation of the selenourea is conveniently monitored by ^{77}Se nuclear magnetic resonance (NMR) spectroscopy, where the chemical shifts of alkyl isoselenocyanates (δ = −345 to −358 ppm)[24] and selenoureas (δ = 175−290 ppm) are distinct (Figure S1). In most cases, the isoselenocyanate does not accumulate and the rate of selenourea formation is limited by the dissolution of elemental selenium, which typically reaches completion over the course of 1 h if 100 mesh selenium powder is used. However, less nucleophilic amines are slower to react and an isoselenocyanate intermediate can be observed. For example, while *n*-butylisoselenocyanate reacts quantitatively with electron-rich 4-methoxy-*N*-methylaniline to form **9** within 35 min, the analogous reaction with *N*-methylaniline proved more sluggish, requiring more than 2 h to reach completion. Even more electron deficient 4-cyano-*N*-methylaniline proved unreactive toward *n*-butylisoselenocyanate over 8 h (Table 2). Sterically bulky derivatives such as *N,N,N′*-tricyclohexylselenourea (**11**) can also be prepared in good yields provided that the amine trapping agent is sufficiently basic.

Table 2. Conversion of Alkyl Isoselenocyanates in the Presence of *N*-Methylanilines (Entries 1−4) and Dialkylamines (Entries 5−6) Determined by ^{77}Se NMR Spectroscopy

	R^1	R^2	R^3	time (h)	conv. (%)
1	*n*-C_4H_9	4-MeO-Ph	Me	1.5	>99
2	*n*-C_4H_9	Ph	Me	2	85
3	*n*-C_4H_9	4-Cl-Ph	Me	3	80
4	*n*-C_4H_9	4-CN-Ph	Me	8	<1
5	*n*-C_4H_9	*n*-C_4H_9	*n*-C_4H_9	0.5	>99
6	Cy	Cy	Cy	0.5	87

Most selenoureas in Table 1 are readily purified by recrystallization and could be structurally characterized using single crystal X-ray diffraction analysis (Figure S2). These structures reveal planar nitrogen atoms, an average C−Se bond length of 1.873 Å, and an average ∠NCN bond angle of 117.2° (Table S1). In all cases, a hydrogen atom was identified on the nitrogen atom and the C−Se bond length fell within the range typical of double bonds. Both features support the selone tautomer, as has been observed in other selenoureas.[25]

While *N,N′*-disubstituted thioureas are appropriately reactive for PbS nanocrystal synthesis,[13] analogous *N,N′*-disubstituted selenoureas (**10**) are too reactive, producing mixing limited kinetics upon injection into lead oleate solution at relatively low temperatures (80 °C). *N,N,N′*-Trisubstituted selenoureas provide slower, controllable conversion reactivity up to 150 °C. Tetrasubstituted selenoureas such as *N,N,N′,N′*-tetramethylselenourea, on the other hand, are not reactive enough to produce soluble PbSe nanocrystals even at relatively high temperature (150 °C). Thus, much like was observed with thioureas, increasing the number of substituents decreases the reactivity of selenoureas toward lead oleate.

PbSe nanocrystals are synthesized by injection of *N,N,N′*-trisubstituted selenoureas dissolved in diphenyl ether, diglyme, or dibutyl ether into a solution of lead oleate in alkane or 1-alkene solvent at 60−150 °C (Figure 1A, S3). The formation of a deep red/brown color occurs 1−50 s following the injection, the timing of which depends on the selenourea structure. Monitoring the UV−vis−NIR spectra of aliquots taken from the reaction mixture shows an increase in the concentration of PbSe and an increase in the average nanocrystal size (Figure S4). Depending on the selenourea structure and temperature, the reaction reaches completion and the nanocrystals approach their final size between 30 s (**12**) and 3 h (**9**) following the injection.

DOI: 10.1021/jacs.6b11021
J. Am. Chem. Soc. 2017, 139, 2296−2305

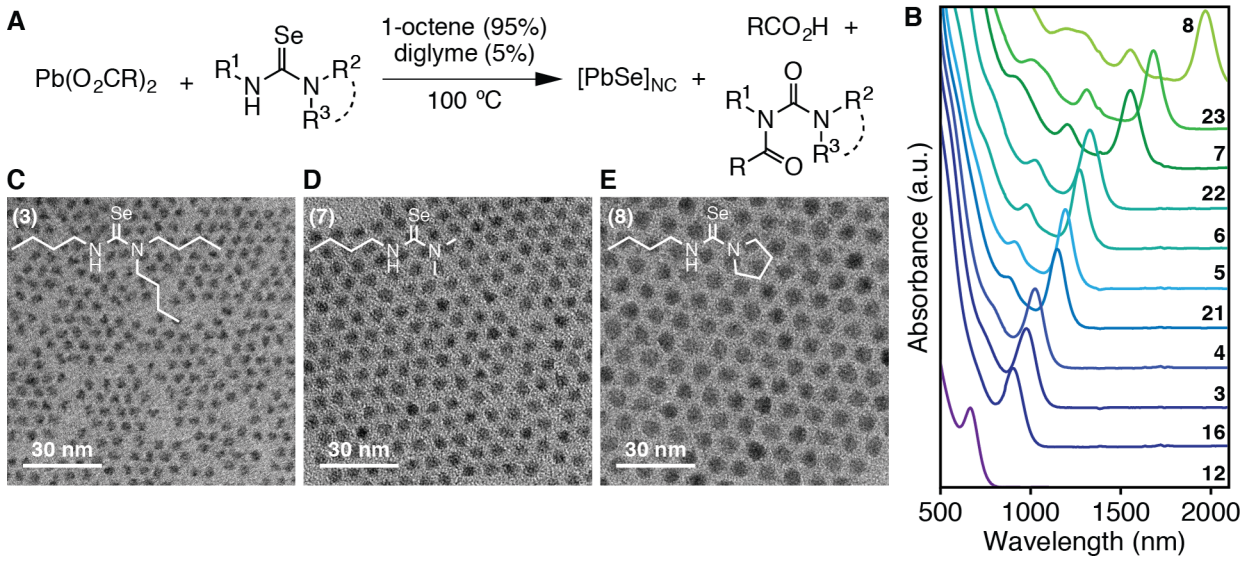

Figure 1. (A) Reaction scheme for the synthesis of PbSe nanocrystals. (B) UV−vis−NIR absorption spectra of aliquots removed from PbSe nanocrystal synthesis reactions at completion using the indicated precursors. (C−E) Transmission electron micrographs of PbSe nanocrystals synthesized from **3**, **7**, and **8**. R = $C_{17}H_{33}$; R^1, R^2, R^3 = alkyl, aryl.

The flexibility of this synthesis platform has allowed us to optimize the crystallization conditions to achieve unusually low polydispersity. By doing so we have arrived at (1) selenourea concentrations of 5−75 mM, (2) lead-to-selenium ratios of 1.2−1.5, where the 20−50% excess lead oleate passivates the surface,[26] and (3) an ideal reaction temperature of 100 °C, where the conversion reactivity is controlled and does not suffer from mixing-limited kinetics, but below which broader spectral line widths can result. To put this temperature in context, 100 °C is considerably lower than those typically used to prepare PbSe from trioctylphosphine selenide (150−180 °C)[27,28] and within the range of temperatures used to synthesize PbSe from secondary phosphine selenide precursors (80−135 °C).[9,10]

The structure of the selenourea reliably dictates the precursor reactivity and the nanocrystal size following complete conversion. The library of structures allows a wide range of nanocrystal sizes to be synthesized (d = 1.7−6.6 nm, $\lambda_{max}(1S_e-1S_h)$ = 615−2000 nm) with line widths indicative of a narrow distribution of sizes (Figures 1B, S5). High-resolution electron microscopies reveal a quasi-spherical shape. (Figures 1C−E, S6). The full-width at half-maximum (fwhm) of the $1S_e-1S_h$ transition ranges from 35−350 meV and decreases with increasing nanocrystal size (see below). At larger sizes (d > 3.9 nm, E_g < 1.0 eV), these spectral line widths are comparable to the best reported literature spectra,[29,30] but the smaller nanocrystals synthesized using selenoureas (d < 3.9 nm, E_g > 1.0 eV), including those that have band gaps relevant for solar cells (E_g > 1.2 eV), have much narrower line widths than previous reports. In the case of more reactive precursors **1** and **11**−**15**, unusually small nanocrystals were obtained (d = 1.6−2.9 nm, E_g = 1.3−2.1 eV) with spectral line widths narrower than any previous example.[31−33]

The kinetics of PbSe formation were monitored in situ using a dip probe to measure the absorbance at λ = 400 nm.[13] At this wavelength the absorbance does not depend on the nanocrystal size and is proportional to the concentration of crystalline PbSe units.[8] Using ^{1}H NMR spectroscopy, clean conversion of the selenourea to the corresponding *N*-acylurea and oleic acid coproducts is observed (Figure 1A, S7). The kinetics of the conversion reaction match the formation of PbSe measured using absorption spectroscopy (Figure S8). Thus, as was concluded in previous studies of PbS,[13] CdSe,[16] CdS,[34] and CdTe,[35] the precursor conversion kinetics can be indirectly monitored by the appearance of the nanocrystal absorption. Example UV−vis absorption kinetics are shown in Figure 2B where the formation of PbSe approaches completion over the course of several minutes to an hour. Following a short induction period preceding crystal nucleation (1−50 s), the evolution of the absorbance at 400 nm is well-described by a single exponential function (Figure 2C, S9) from which we extract a rate constant (k_{obs}, sec^{-1}).

By normalizing the k_{obs} to the slowest precursor (**26**), a series of relative conversion rate constants (k_{rel}) are obtained that can be used to assess the effect of the selenourea structure on the conversion reactivity. For example, increasing the steric bulk of the substituents increases the k_{rel} over more than 3 orders of magnitude (Figure 2C). A similar increase in the reactivity of thioureas with increasing steric bulk suggests that elimination of lead sulfide and lead selenide from a chalcogenoureate complex may be involved in the rate-determining step.[13] It is interesting to note that pyrrolidine-derived selenoureas are relatively unreactive compared to di-*n*-alkyl derivatives. We attribute the decreased reactivity to the more acute C−N−C substituent bond angle of the five-membered pyrrolidine ring (**23**, Figure S2L), which lowers its steric encumbrance. Consistent with this hypothesis, the analogous selenourea derived from piperidine (**15**, Figure S2D) has a wider C−N−C angle within the ring and converts at a faster rate. Aryl-substituted selenoureas (**24**−**26**, **9**) react an order of magnitude more slowly than their alkyl analogues (**18**, **22**). Similarly, *N,N,N′*-trisubstituted *thioureas* with aryl-substituents are less reactive toward cadmium oleate than the aliphatic analogues.[13] However, this substituent trend is reversed in reactions between *N,N′*-disubstituted thioureas and lead oleate where aryl substituents increase the reactivity of toward lead oleate. This signals a change in the rate limiting step from deprotonation of the thiourea or nucleophilic attack at the thione carbon, as was suggested earlier for *N,N′*-

DOI: 10.1021/jacs.6b11021
J. Am. Chem. Soc. 2017, 139, 2296−2305

A

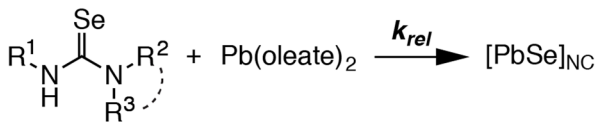

C

	R¹	R²	R³	T (°C)	k_{rel}
12	Cy	^{i}Pr	^{i}Pr	60	**12000**
13	Cy	^{i}Pr	Et	60	**960**
14	Cy	^{i}Pr	Me	60	**350**
15	Cy	–$(CH_2)_5$–		80	**260**
16	Cy	*n*-C_4H_9	*n*-C_4H_9	60, 80	**110**
17	Cy	Et	Et	80	**110**
3	*n*-C_4H_9	*n*-C_4H_9	*n*-C_4H_9	80	**71**
18	Cy	Et	Me	80	**36**
5	*n*-C_4H_9	*n*-C_4H_9	Me	80	**21**
19	Cy	-2-Me-$(CH_2)_4$-		80	**20**
21	Cy	Allyl	Allyl	80	**14**
22	Cy	Me	Me	80, 90	**13**
23	Cy	–$(CH_2)_4$–		90, 110	**2.7**
24	Cy	4-MeO-Ph	Me	110, 120	**1.9**
25	Cy	Ph	Me	120	**1.0**
26	Cy	4-Cl-Ph	Me	120	**1.0**
8	*n*-C_4H_9	–$(CH_2)_4$–		110	**1.8**
9	*n*-C_4H_9	4-MeO-Ph	Me	110	**1.2**

B

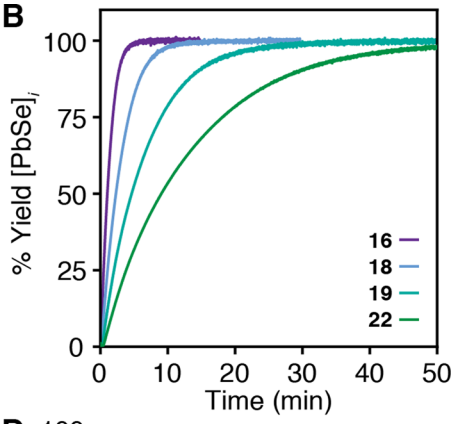

D

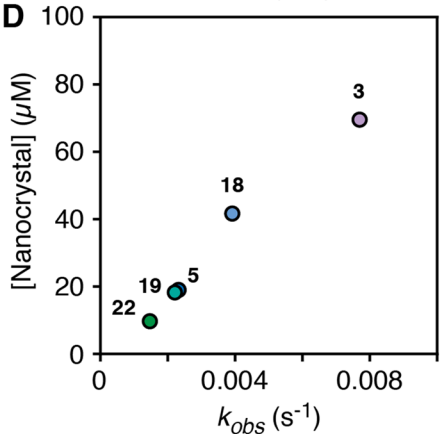

Figure 2. (A) Kinetic studies of PbSe formation from the reaction of lead oleate and selenoureas at 60–120 °C. (B) Kinetics of PbSe formation as measured in situ by the absorbance at λ = 400 nm. (C) Effect of substituents on the relative single exponential rate constants. $k_{rel}(i)$ was calculated by dividing the measured rate constant for precursor ***i*** by the rate constant for the slowest selenourea, k_{rel}(**26**) (e.g. k_{rel}(**24**) = k(**24**)/k(**26**)). The wide range of reactivity requires that kinetics are measured at multiple temperatures. To account for the temperature dependence of the conversion rate constant, **16** and **22**–**24** were measured at two temperatures, and the change in rate constant was used to normalize the relative rate constants of the respective temperatures (e.g., k_{rel}(**8**) = [k(**8**)$^{110\ °C}$/k(**24**)$^{110\ °C}$] × [k(**24**)$^{120\ °C}$/k(**26**)$^{120\ °C}$]. Precursors **8**, **15**, **19**, and **23** contain cyclic amino substituents (e.g. piperidino, pyrrolidino, 4-methylpyrrolidino) as indicated by the dashed line in **A**. (D) Nanocrystal concentration versus rate constant (k_{obs}) of PbSe formation at 80° for **3**, **5**, **18**, **19**, and **22**. Reported k values are averages of three trials.

disubstituted thioureas,[13] to a rate limited by elimination of the metal chalcogenide from a chalcogenoureate complex.

Following the nucleation mass balance described by Sugimoto,[15] the number of nanocrystals produced by nucleation (n_f, L^{-1}) is determined by the solute supply rate (Q_o, mol L^{-1} s^{-1}) and the nucleus growth rate (v_n, nm^3 L^{-1} s^{-1}), where V_m is the molar volume (nm^3 mol^{-1}) of a PbSe crystal monomer (eq 1).

$$n_f = \frac{Q_o V_m}{v_n} \quad (1)$$

Consistent with this theory and previous studies of AgCl,[15] AgBr,[14] CdSe,[16,17] CdS,[13] and PbS,[13] we find that faster selenourea conversion kinetics result in larger n_f and smaller final nanocrystal sizes. This correlation is caused by changes to the extent of nucleation and is not affected by Ostwald ripening, which is negligibly slow under our conditions (Figure S10). The k_{obs} values extracted from PbSe formation kinetics are plotted versus the resultant nanocrystal concentrations in Figure 2D, where a linear correlation between the conversion reactivity and the nanocrystal concentration can be observed. From the slope of the plot we extract a nucleus growth rate v_n of 0.94 PbSe units/sec according to eq 1. Using this growth rate and the size distributions extracted below, we estimate the length of the nucleation period to be on the order of 3–16 s.

The library of conversion reactivity also allows the reaction temperature and precursor to be independently optimized to obtain a desired result. For example, by choosing the appropriate precursor, mixing-limited kinetics during the injection are avoided at large reaction scales (1–5 g) (Figures 3B, S11, 12). This allowed us to develop a large scale synthesis of nanocrystals with a band gap appropriate for the fabrication of photovoltaic devices ($\lambda_{max}(1S_e–1S_h)$ = 985–1015 nm). Moreover, low-boiling solvents (bp(1-octene) = 122 °C; bp(Bu_2O) = 142 °C; bp(diglyme) = 162 °C, respectively) can be chosen that are then easily distilled from the crude nanocrystal product, facilitating the isolation process on large scale. Complete conversion of the starting materials leaves a final reaction mixture whose composition is defined by the starting ratios of reactants, thereby allowing a standard purification procedure to be developed that reproducibly produces nanocrystals with a known ligand coverage (Table S2, Figure S13). Optimized isolation procedures that provide reproducible chemical compositions are especially important in light of the reversible surface passivation provided by metal carboxylates, which bind the nanocrystal and influence the photoexcited carrier recombination.[26,36]

DOI: 10.1021/jacs.6b11021
J. Am. Chem. Soc. 2017, 139, 2296–2305

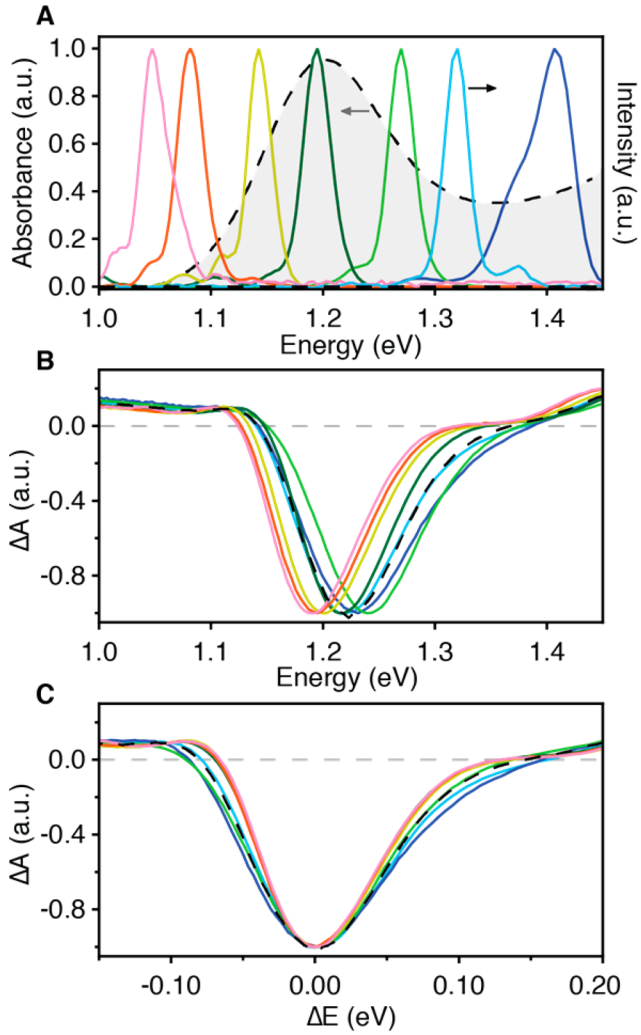

Figure 3. (A) Nanocrystal extinction spectrum for an ensemble with E_g = 1.2 eV (dashed black line) and the spectra of the laser pulses used for photoexcitation. (B) Transient spectra recorded at t = 2 ns as a function of photon energy. (C) Transient spectra as a function of photon energy, offset to account for changes in the ground state bleach minima.

The size distribution of colloidal nanocrystals is often estimated by analyzing the spectral line width of the first optical transition. However, this analysis typically assumes the intrinsic line width of a single size is much lower than broadening caused by the size distribution.[34,37,38] Recent measurements suggest that exciton−phonon coupling, spectral diffusion, and exciton fine structure can account for more than 50% of the room temperature ensemble line width in highly monodisperse samples, which is at odds with the aforementioned assumption.[39−41] Moreover, photoluminescence correlation measurements,[40] photon-echo techniques,[42] single-dot spectroscopy,[43,44] and the absorption spectra of atomically precise clusters[45] show a decreasing intrinsic line width as the size increases in CdSe and PbS nanocrystals increase. Thus, in samples of colloidal crystals with narrow size distributions the spectral line width of the ensemble depends on both the intrinsic line width of single particles, the particle size, and the size distribution.

Given the narrow size distributions evident from the sharp spectral features in Figure 1B, we sought to estimate the single-particle spectral line width using transient spectral hole burning measurements.[46] Wavelength-tunable excitation pulses that are narrower than the $1S_e-1S_h$ line width of our samples (5−40 meV versus 65−320 meV) were used to selectively excite a fraction of the ensemble. Following pump−probe delay times (t = 2 ns) that are much longer than multiexciton lifetimes, we measure induced changes in the absorption spectrum (ΔA) as a function of the pump wavelength. Typical transient absorption (TA) spectra for an ensemble with E_g = 1.2 eV are plotted in Figure 3. As the excitation pulse is tuned from the tail of the $1S_e-1S_h$ absorption, where only the largest nanocrystals absorb, to higher energies, we observe a corresponding shift in the minimum of the ground state bleach signal (Figure 3B). After accounting for this shift (Figure 3C) and the finite spectral width of the excitation pulses (see Experimental Section),[46] we deconvolute the transient absorption spectrum to determine the average single particle transient absorption line width. In all cases, this width is 17−27% narrower than that of the ensemble excited far above the band edge. We therefore estimate that the average single particle line width of the $1S_e-1S_h$ transition in the steady state absorption spectrum is 73−83% of the ensemble line width and conclude that the broadening due to the size distribution accounts for the remaining 17−27%. Using the percent narrowing measured with TA, we calculate the intrinsic absorption line widths of single sizes and plot them next to the ensemble line widths in Figure 4A (see also: Figure S14). A recent measurement of the intrinsic average single PbSe particle line width ($1S_e-1S_h$ = 1.1 eV, fwhm = 80 meV) was performed using two-dimensional Fourier transform spectroscopy, and is in good agreement with our measurements.[47]

A significant decrease in the broadening is evident as the size of the nanocrystal increases. The broadening derives mainly from two effects: fine structure in the electronic states and exciton−phonon coupling. Tight binding calculations on a series of PbSe particle sizes indicate that broadening caused by fine structure, including intervalley coupling, is size dependent and can account for roughly half the observed broadening in Figure 4.[48−52] The remainder can be attributed to thermal broadening such as exciton phonon coupling, which is predicted to be stronger in small nanocrystals, although some disagreement exists over the magnitude of its size dependence.[53−57] Regardless of the source of the intrinsic spectral broadening, the data clearly show that the broadening caused by the size distribution is minor across the wide range of sizes accessible with the selenourea library.

Mechanistic studies of nanocrystal growth often use the spectral line width to argue for or against a particular growth mechanism: e.g., spectral broadening with increasing size is signature of Ostwald ripening, while spectral narrowing is signature of size distribution focusing. However, the size dependence of the single particle line width evident in Figure 4 and in other studies[58,59] must be considered in order to correctly extract the size distribution. In particular, the numerous claims of size distribution focusing should be reevaluated in light of our finding as well as related work on CdSe and PbS nanocrystals.[37] In the present case, the spectral line width is mostly a consequence of the intrinsic broadening of a single size and is not significantly influenced by the size distribution. Indeed, our estimate indicates that the relative standard deviation in the nanocrystal diameter is 0.5−2% for all samples studied here, corresponding to total distributions in the formula of 3−15 PbSe units, assuming a spherical particle

DOI: 10.1021/jacs.6b11021
J. Am. Chem. Soc. 2017, 139, 2296−2305

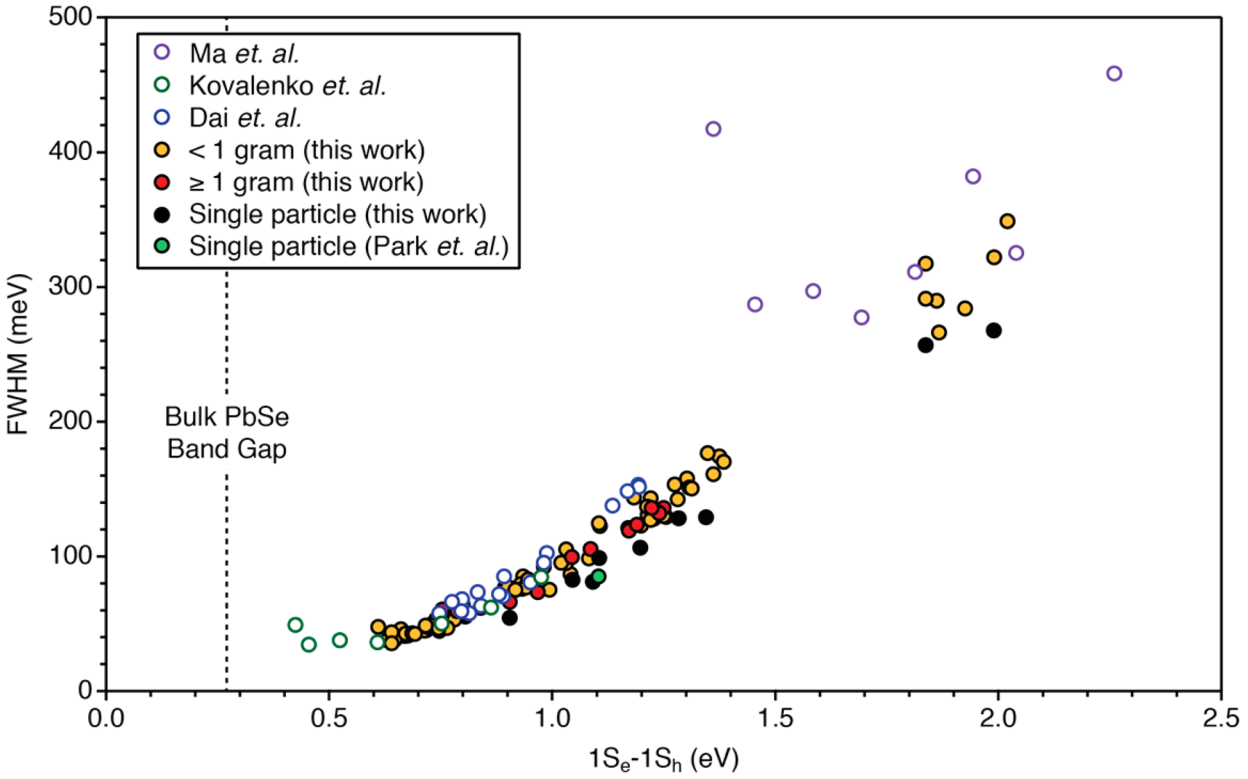

Figure 4. Results of a reproducibility study showing the fwhm of the lowest energy electronic transition versus its position ($1S_e-1S_h$) across 94 reactions using a variety of selenourea precursors and reaction scales (yellow, red). These data are overlaid with data extracted from previously published spectra of PbSe samples (violet,[31] green,[29] blue[30]) and single-particle component line widths (black, green/black).

shape. These distributions are vanishingly small and unlikely to induce significant differences in the relative growth rates of different radii within the size distribution.[59]

CONCLUSIONS

We report a library of *N,N,N′*-trisubstituted selenoureas whose conversion kinetics to PbSe nanocrystals can be finely controlled by adjusting their substitution pattern. The nanocrystal concentration and therefore the final nanocrystal size following complete precursor conversion are readily tuned by the conversion reactivity. These precursors provide a convenient synthesis of PbSe nanocrystals on large reaction scales whose spectral features are exceptionally narrow and dominated by single-particle spectral broadening rather than the size distribution. This is especially valuable at small sizes where it has proven difficult to access PbSe nanocrystals whose band gap is appropriate for solar photovoltaic devices.

EXPERIMENTAL SECTION

General Methods. All manipulations were performed using standard air-free techniques on a Schlenk line under argon atmosphere or in a nitrogen-filled glovebox unless otherwise indicated.

Chemicals. Acetonitrile (≥99.5%), hexane (mixture of isomers, ≥98.5%), isopropanol (≥99.5%), methanol (≥99.8%), and toluene (≥99.5%) were obtained from Aldrich and used without further purification. Tetrachloroethylene (anhydrous, ≥99%), tetrahydrofuran (anhydrous, ≥99.9%, inhibitor-free), methyl acetate (99.5%, anhydrous), decane (anhydrous, ≥99%), dibutyl ether (anhydrous, 99.3%), diethylene glycol dimethyl ether ("diglyme", anhydrous, 99.5%) were obtained from Aldrich, transferred to a glovebox, shaken with activated alumina, filtered, and stored over activated 3 Å molecular sieves for 24 h prior to use. Toluene (≥99.5), dichloromethane (≥99.5%, contains 40−150 ppm amylene as stabilizer), and diethyl ether (≥99.9%, inhibitor-free) were obtained from Aldrich, degassed, dried in a column packed with activated alumina, and stored in a glovebox over activated 3 Å molecular sieves for 24 h prior to use. Pentane (≥98%) was obtained from Fisher Chemical, degassed, dried in a column packed with activated alumina, and stored in a glovebox over activated 3 Å molecular sieves for 24 h prior to use. Diphenyl ether (≥99%), hexadecane (99%), and *n*-octane (≥99%) were obtained from Aldrich, stirred with calcium hydride overnight, distilled and stored in a glovebox over activated 3 Å molecular sieves for 24 h prior to use. 1-octene (99%) was obtained from Acros Organics, stirred with calcium hydride overnight, distilled and stored in a glovebox over activated 3 Å molecular sieves for 24 h prior to use. Benzene-d_6 (*d*, 99.5%), chloroform-*d* (*d*, 99.8%), dichloromethane-d_2 (*d*, 99.8%), tetrahydrofuran-d_8 (*d*, 99.5%), and toluene-d_8 (*d*, 99.5%) were obtained from Cambridge Isotope Laboratories and stored in a glovebox over activated 3 Å molecular sieves for 24 h prior to use.

Diisopropylamine (≥99.5%), dibutylamine (≥99.5%), diethylamine (≥99.5%), pyrrolidine (≥99.5%, purified by distillation), piperidine (≥99.5%, purified by distillation), *N*-*n*-butylmethylamine (96%), diallylamine (99%), dimethylamine (2.0 M in tetrahydrofuran), Dicyclohexylamine (99%), *N*-ethylisopropylamine (98%), *N*-isopropylmethylamine (98%), *N*-ethylmethylamine (97%), 1,2,3,4-tetrahydroisoquinoline (95%), 4-chloro-*N*-methylaniline (97%), and *N*-methylaniline (98%) were obtained from Aldrich, stirred with calcium hydride overnight, distilled and stored in a glovebox. 2-methylpyrrolidine (98%) was obtained from Acros Organics, stirred with calcium hydride overnight, distilled and stored in a glovebox. 4-methoxy-*N*-methylaniline (98%) was obtained from Combi-Blocks, stirred with calcium hydride overnight, distilled and stored in a glovebox. Dimethyl terephthalate (≥99%), tris(dimethylamino)methane (97%), 4-(methylamino)benzonitrile (97%), and triethylamine (≥99%) were obtained from Aldrich and used without further purification. Selenium (100 mesh, 99.99%) and phosphorus(V) oxychloride (99%) were obtained from Aldrich and used without further purification. Lead(II) oxide (99.999+%) was obtained from Strem or Alfa Aesar and used without further purification. Cyclohexyl isocyanide (99%), *n*-butyl

DOI: 10.1021/jacs.6b11021
J. Am. Chem. Soc. 2017, 139, 2296−2305

isocyanide (98+%), and *tert*-butyl isocyanide (97%) were obtained from Acros Organics, degassed by the freeze−pump−thaw method, and stored in a glovebox. Trifluoroacetic acid (99%) and trifluoroacetic anhydride (99%) were obtained from Aldrich and used without further purification. *N*-*n*-hexadecylformamide (97%) was obtained from Alfa Aesar and used without further purification. Oleic acid (99%) was obtained from Aldrich or Alfa Aesar, stored in a −20 °C freezer, and used without further purification.

Instrumentation. UV−vis−NIR spectra were obtained using a PerkinElmer Lambda 950 spectrophotometer equipped with deuterium and halogen lamps and either a PbS or InGaAs detector. Samples for UV−vis−NIR and photoluminescence spectroscopies were dissolved in tetrachloroethylene. A background spectrum was obtained of the same solvent mixture and concentration as the sample to be analyzed. Infrared photoluminescence measurements were conducted using excitation from a 6 ps supercontinuum laser. After spectral filtering, the excitation light (590 ± 10 nm, < 25 nJ cm^{-2} per pulse) was focused onto a dilute solution of nanocrystals. The emission was collected using reflective optics, dispersed by a 1/3-m spectrometer, and detected with an InGaAs photodiode and lock-in amplifier. The grating angle was scanned to acquire spectra. All spectra were corrected for grating and detector efficiency, and the measurements were conducted under inert atmosphere with weak excitation and stirring to prevent experimental artifacts due to oxidation, multiple excitation, and photocharging.

NMR spectroscopy was performed on Bruker 300, 400, and 500 MHz spectrometers. ^{77}Se NMR spectra were referenced to diphenyl diselenide in benzene-d_6 (464.10 ppm[60]), which was sealed inside a glass capillary and placed inside the NMR tube. Single crystal XRD analysis was performed on either an Agilent SuperNova SCXRD or a Bruker Apex II diffractometer. Powder XRD analysis was performed on a Scintag X-ray diffractometer. Transmission electron microscopy (TEM) was performed on either a JEOL JEM-100CX or a JEOL 2100 TEM. High-resolution TEM images were recorded on a FEI Talos F200X, operated at 200 kV without a C_s corrector. STEM images were recorded at a nominal spot size of 9 and a 50 μm condenser aperture.

Kinetics experiments were carried out under nitrogen at 9 mM in selenourea according to Hendricks et al.[13] Kinetics experiments were monitored at 400 nm using a PerkinElmer 316SS dip probe (2 mm path length) attached to a PerkinElmer Lambda 650 spectrophotometer equipped with deuterium and halogen lamps.

Transient spectral hole burning experiments were performed using a commercial amplified Ti:sapphire laser system (SpectraPhysics) operating at a repetition rate of 1 kHz. Resonant excitation pulses were generated by a collinear optical parametric amplifier (LightConversion) and the spectrum of each pulse was measured using a fiber coupled commercial miniature spectrometer (Ocean Optics NIRQuest). Near-infrared supercontinuum probe light was generated using a sapphire plate. Cross-polarized pump and probe beams were used to reject the scattered pump light. Transient spectra were recorded on a shot-by-shot basis using a pair of fiber coupled InGaAs (infrared) diode arrays (Ultrafast Systems). The excitation fluence in each measurement was approximately 100 $\mu J/cm^2$.

Precursor Synthesis. Lead oleate was prepared from lead trifluoroacetate according to Hendricks et al.[13] on 134 mmol scale. It is important to use high-purity, yellow lead(II) oxide in this reaction. *n*-Hexadecyl isocyanide was prepared according to Hoertz et al.[61] at 40 mmol scale. *N*,*N*,*N*′,*N*′-tetramethylselenourea was prepared according to Kantlehner, Hauber, and Vettel.[62]

Synthesis of Selenoureas 1−31. In a glovebox, selenium (3.0 mmol), amine (3.0 mmol), isocyanide (3.0 mmol), and toluene (to a total volume of 3 mL) are sealed under nitrogen and the mixture stirred in an oil bath heated to 100 °C for 1 h. During this time nearly all of the selenium is consumed and the reaction mixture becomes colorless to yellow. The vessel is then transferred to a glovebox and, mixture is passed through a syringe filter (PTFE, 0.2 μm), and the volatiles are removed under vacuum. Solid selenoureas are recrystallized using solvents indicated in the Supporting Information, isolated by filtration using a glass fritted funnel, and dried under vacuum for >3 h. Liquid and low-melting solid selenoureas area placed under vacuum for 24 h with stirring. Isolated selenoureas are stored at −40 °C in a glovebox freezer where they are indefinitely stable. All reactions were performed at a 3.0 mmol scale unless otherwise noted, but can be run at 25 times the scale and twice the above concentrations without significantly impacting the results.

Example Selenourea Synthesis. *N,N-Dibutyl-N′-cyclohexylselenourea (**16**).* *N*,*N*-Dibutyl-*N*′-cyclohexylselenourea is prepared according to the general procedure from dibutylamine (387.7 mg, 3.00 mmol), selenium (236.9 mg, 3.00 mmol), and cyclohexyl isocyanide (327.5 mg, 3.00 mmol) in toluene (2.6 mL). The filtrate is recrystallized by concentration of a saturated solution in toluene under reduced pressure. The solid is isolated by suction filtration on a fritted glass funnel, washed with pentane (3 × 4 mL), and dried under vacuum for >3 h. White solid. Yield: 727.2 mg (76.4%).

Example Selenourea Synthesis. *N′-Cyclohexyl-N-ethyl-N-methylselenourea (**18**).* *N*′-Cyclohexyl-*N*-ethyl-*N*-methylselenourea was prepared according to the general procedure from *N*-ethylmethylamine (177.3 mg, 3.00 mmol), selenium (236.9 mg, 3.00 mL), and cyclohexyl isocyanide (327.5 mg, 3.00 mmol) in toluene (2.6 mL). Pentane (6 mL) is added to the filtrate to induce crystallization, and then the mixture is cooled in a −40 °C freezer for >2 h. Following this period, the crystals are isolated by suction filtration on a fritted glass funnel, washed with pentane (3 × 4 mL), and dried under vacuum >3 h. Pale yellow crystals. Yield: 510.6 g (68.8%).

Example Selenourea Synthesis. *N,N-Diallyl-N′-butylselenourea (**6**).* *N*,*N*-Diallyl-*N*′-butylselenourea was prepared according to the general procedure from diallylamine (291.5 mg, 3.00 mmol), selenium (236.9 mg, 3.00 mmol), and butyl isocyanide (249.4 mg, 3.00 mmol) in toluene (2.6 mL). Pale yellow, nearly colorless oil. Yield: 757.2 mg (97.4%).

Synthesis of PbSe Nanocrystals for Absorbance and Photoluminescence Spectroscopies. In a glovebox, lead oleate (231.0 mg, 0.30 mmol, 1.5 equiv) and 1-octene (9.5 mL) are added to a 40 mL scintillation vial equipped with a stir bar that is then sealed with a rubber septum. The selenourea (0.20 mmol) and diglyme (0.5 mL) are added to a 4 mL scintillation vial and sealed with a rubber septum. Both vials are removed from the glovebox, the septa pierced with argon inlet needles, and placed in oil baths at 100 °C. After reaching thermal equilibrium (15 min), the selenourea solution is injected into the lead oleate solution. An aliquot (100 μL) is removed at the desired time and dissolved in tetrachloroethylene (6 mL) for absorbance spectroscopy. For photoluminescence measurements, the reaction mixture is transferred via syringe into a Schlenk flask under argon, brought into a glovebox, and diluted in tetrachloroethylene to an absorbance of 0.1−0.3 at the $1S_e-1S_h$ maximum.

Large-Scale Synthesis of 2.7 nm PbSe Nanocrystals. In a glovebox, lead oleate (2.657 g, 3.45 mmol, 1.5 equiv) and 1-octene (54.6 mL) are added to a 100 mL 3-neck round-bottom flask equipped with a stir bar, that is then sealed with two rubber septa and an air-free vacuum adapter. In a 20 mL scintillation vial, *N*,*N*-dibutyl-*N*′-cyclohexylselenourea (0.730 g, 2.30 mmol) and dibutyl ether (2.9 mL) are mixed and the vial sealed with a rubber septum. Both vessels are transferred to a Schlenk line where they are placed under nitrogen and brought to 100 °C in an oil bath. Once the temperature is stable, the solution of selenourea is quickly injected into the clear colorless solution of lead oleate via a syringe equipped with a wide gauge needle. The reaction is allowed to run for 10 min before the flask is removed from the oil bath and allowed to cool to room temperature. The septa are then replaced with glass stoppers under positive argon flow and the volatiles removed under vacuum. After 3 h, the flask is sealed and transferred to a nitrogen-filled glovebox. The dark residue is dissolved in 12 mL of a 1:1 pentane/toluene mixture. 50 mL of methyl acetate are added to precipitate the nanocrystals and the mixture is centrifuged (7000 rpm, 10 min), giving a clear, pale brown supernatant. The dark residue remaining is dissolved in 12 mL of a 1:1 pentane/toluene mixture, precipitated with 50 mL of methyl acetate, and centrifuged (7000 rpm, 10 min). This process is repeated three more times (five precipitations in total), and then the nanocrystal solution is dried under vacuum for >6 h. The nanocrystal solid is dissolved in benzene-d_6 or toluene-d_8 for analysis with UV−vis−NIR and NMR spectros-

DOI: 10.1021/jacs.6b11021
J. Am. Chem. Soc. 2017, 139, 2296−2305

copies. Yield: 83−97%, based on empirical formulas of (PbSe)(Pb(oleate)$_2$)$_n$ determined spectroscopically. Commercially available anhydrous octane (bp = 125−126 °C) may also be used in place of 1-octene.

Large-Scale Synthesis of 5.1 nm PbSe Nanocrystals. In a glovebox, lead oleate (10.497 g, 13.63 mmol, 1.2 equiv) and 1-octene (146 mL) are added to a 250 mL 3-neck round-bottom flask equipped with a stir bar, that is then sealed with two rubber septa and an air-free vacuum adapter. To a 20 mL scintillation vial, *N*,*N*-diallyl-*N*′-butylselenourea (2.945 g, 11.36 mmol) and diglyme (5 mL), were added and the vial sealed with a rubber septum. Both vessels are transferred to a Schlenk line where they are placed under nitrogen and brought to 100 °C in an oil bath. Once the temperature is stable, the solution of selenourea is quickly injected into the clear colorless solution of lead oleate. The reaction is stirred for 120 min before the flask is removed from the oil bath and allowed to cool to room temperature. The septa are then replaced with glass stoppers under positive argon flow and the volatiles removed under vacuum. After 2 h, the flask is placed under argon and the glass stoppers replaced with rubber septa. 50 mL of pentane is then added via cannula, and the dark slurry was transferred via cannula to a Teflon-sealable Schlenk flask and taken into a nitrogen glovebox. 70 mL of methyl acetate was added and the mixture was centrifuged (7000 rpm, 10 min.), giving a clear, pale brown supernatant. The dark residue remaining was dissolved in 65 mL of a 1:1 pentane/toluene mixture, precipitated with 135 mL of methyl acetate, and centrifuged (7000 rpm, 10 min.). The process of precipitation, centrifugation, and redissolution was repeated three more times. The nanocrystal solution was then dried under vacuum for 24 h and the solid dissolved in a mixture of tetrachloroethylene and benzene-d_6 or toluene-d_8 for analysis with UV−vis−NIR and NMR spectroscopies. Commercially available anhydrous octane (bp = 125−126 °C) may also be used in place of 1-octene.

Rate of Ostwald Ripening Experiment. Ostwald ripening was determined to be negligibly slow by following the same procedure described for the synthesis of PbSe nanocrystals for absorbance and photoluminescence spectroscopies. *N*,*N*-diallyl-*N*′-butylselenourea was injected into the lead oleate solution at 100 °C. Aliquots (200 μL) were removed at 2, 5, and 8 h after injection and dissolved in tetrachloroethylene (6 mL) for absorbance spectroscopy.

Determination of Oleate, PbSe, and Nanocrystal Concentrations. The concentration of oleate in a given nanocrystal sample is determined by ^{1}H NMR spectroscopy. Purified nanocrystals are thoroughly dried under vacuum and dissolved in benzene-d_6 or toluene-d_8. Dimethyl terephthalate (DMT) dissolved in benzene-d_6 or toluene-d_8 (100 μL, 50.1 mM) was added to a known volume of the nanocrystal stock solution and its aromatic resonances used as an internal standard for ^{1}H NMR spectroscopy. The concentration of ligands was determined relative to the DMT internal standard by integrating the ligand vinyl and DMT aryl resonances and normalizing for the number of hydrogens, respectively (2:4). ^{1}H NMR spectra were acquired with sufficient relaxation delay to allow complete relaxation between pulses (T1(oleate vinyl) = 1.0 s; T1(DMT aryl) = 12.0 s; 5 × T1 = 60 s). See Figure S13 for an example ^{1}H NMR spectrum of isolated PbSe nanocrystals.

The concentration of nanocrystals was determined by UV−vis−NIR absorbance spectroscopy. The molar concentration of PbSe in these stock solutions was determined by diluting 10−50 μL to a known volume with tetrachloroethylene and measuring the absorbance at λ = 400 nm. At this wavelength, the extinction coefficient is independent of size:[8]

$$[\mathrm{PbSe}] = \frac{A_{400}}{\varepsilon_{400} l}$$

The wavelength of the lowest energy absorption maximum was used to determine the average nanocrystal diameter.[30] Assuming the nanocrystals have a spherical shape and the molar volume of bulk PbSe ($0.0584925 N_A$), the number of PbSe units per nanocrystal was calculated from the nanocrystal diameter. The concentration of nanocrystals is determined by dividing the concentration of PbSe by the number of PbSe formula units per nanocrystal.

The number of ligands per nanocrystal is determined by dividing the ligand concentration measured by ^{1}H NMR by the nanocrystal concentration measured by UV−vis−NIR and the ligand surface density is calculated by dividing the number of ligands per nanocrystal by the average surface area per nanocrystal.

Estimation of Single-Particle Line Widths. To estimate the line widths of the nanocrystal electronic transitions, we use a modified version of the transient spectral hole burning experiments described in Norris et al.[46] Briefly, features in the t = 2 ns transient absorption spectra are fit using a negative amplitude Gaussian function bordered by two positive amplitude Gaussian functions. The positive functions account for spectral shifts associated with the excited state of the quantum dot (also known as the biexciton effect).[46,63,64] A linear baseline was used to account for the background photoinduced absorption signals. A typical spectral decomposition is shown in Figure S15 and a typical time dependence is shown in Figure S16. In all cases, the line width of the transition is taken to be the width of the negative Gaussian signal component (with variance $\sigma^2_{\mathrm{measured}}$).

We account for the finite width of the laser pulse spectrum using by fitting it to a Gaussian line shape (whose variance is $\sigma^2_{\mathrm{laser}}$). Deconvolution is used to obtain the corrected line widths (with variance of $\sigma^2_{\mathrm{particle}}$) as a function of excitation energy:

$$\sigma^2_{\mathrm{measured}} = \sigma^2_{\mathrm{laser}} + \sigma^2_{\mathrm{particle}}$$

The finite bandwidth of the laser pulse minimally affects the measured line width. For the sample with E_g = 1.2 eV shown in the main text, the measured and deconvoluted line widths differ by only 5%. This is a typical value for the range of samples reported here (2−7% difference). The high excitation energy ensemble line width is independent of the laser pulse spectrum since the spectrum is featureless and absorbs roughly equally over the excitation pulse width in that spectral region. As such, no deconvolution of the laser line shape is used to determine the ensemble widths (extracted using the Gaussian fitting procedure described above).

The $1S_e$−$1S_h$ transition is fit to a Gaussian function on an eV scale. The resulting c (width) parameter is multiplied by the percent narrowing obtained from spectral hole burning measurements, giving the homogeneous line width c_0. The inhomogeneous broadening is expressed as $c - c_0$ (in eV) and plotted in Figure 4 in the main text.

Estimation of Relative Standard Deviation (%RSD). The absorption spectrum is converted to nanocrystal diameter according to Dai et al.:[30]

$$d = (\lambda - 143.75)/281.25$$

where d is the nanocrystal diameter in nanometers. The $1S_e$−$1S_h$ transition within this plot is fit to a Gaussian function and from which c is multiplied by the percent narrowing obtained from spectral hole burning measurements, giving the single-particle line width c_0 (in nm). These parameters are used to obtain a relative (%) standard deviation in diameter:

$$\%\mathrm{RSD} = \frac{c - c_0}{d}$$

where d is the average nanocrystal diameter. d is also converted to a number of PbSe formula units per nanocrystal at each point:

$$n_{\mathrm{PbSe}} = \frac{V_{\mathrm{NC}} Z}{V_{\mathrm{UC}}} = \frac{\pi d^3 Z}{6 V_{\mathrm{UC}}}$$

where n_{PbSe} is the average number of PbSe formula units per nanocrystal, V_{NC} is the average nanocrystal volume in nm^3 (assuming sphericity), Z is the number of PbSe formula units per unit cell (Z = 4 for rock salt PbSe), and V_{UC} is the volume of the PbSe unit cell (0.0584925 nm^3). The c parameter extracted from Gaussian fit on this axis is multiplied by 1 minus the percent narrowing obtained from spectral hole burning measurements, giving the homogeneous line width c_0 in terms of n_{PbSe}. The inhomogeneous broadening is again

DOI: 10.1021/jacs.6b11021
J. Am. Chem. Soc. 2017, 139, 2296−2305

expressed as $c - c_0$, giving the standard deviation in n_{PbSe}. These values are plotted in Figures 4B and 4C in the main text.

■ ASSOCIATED CONTENT

Supporting Information

The Supporting Information is available free of charge on the ACS Publications website at DOI: 10.1021/jacs.6b11021.

NMR spectra, UV−vis−NIR spectra, photoluminescence spectra, kinetics data, reproducibility plots, surface ligand coverage calculations, hole burning spectra and fits, precursor characterization, and crystallographic data (PDF)

CIF files (ZIP)

■ AUTHOR INFORMATION

Corresponding Authors

*msfeir@bnl.gov

*jso2115@columbia.edu

ORCID

Michael P. Campos: 0000-0003-1568-2561

Zeger Hens: 0000-0002-7041-3375

Matthew Y. Sfeir: 0000-0001-5619-5722

Jonathan S. Owen: 0000-0001-5502-3267

Notes

The authors declare no competing financial interest.

■ ACKNOWLEDGMENTS

The precursor library development and reaction kinetics were supported by the National Science Foundation under grant CHE-1151172. Large-scale synthesis and surface ligand analysis was supported by the Department of Energy under grant DE-SC0006410. Evelyn Auyeung performed transmission electron microscope measurements on a JEOL 2100 instrument. Ilan Jen-La Plante performed transmission electron microscope measurements on a JEOL 2100F instrument at the New York Structural Biology Center (NYSBC). NYSBC is supported by NYSTAR and the Research Facilities Improvement Program C06 RR017528-01-CEM from the National Center for Research Resources, National Institutes of Health. We thank J. Palmer and G. Parkin for assistance with X-ray crystallography and the National Science Foundation (CHE-0619638) for acquisition of an X-ray diffractometer. We thank Daniel W. Paley for helpful discussions regarding crystallography and Columbia University's Shared Materials Characterization Lab for the use of X-ray equipment essential to this research. We thank E. Busby for assistance with NIR photoluminescence. This research used resources of the Center for Functional Nanomaterials, which is a U.S. DOE Office of Science Facility, at Brookhaven National Laboratory under Contract No. DE-SC0012704. WW acknowledges funding from the European Union's Framework Programme for Research and Innovation Horizon 2020 (2014-2020) under the Marie Skłodowska-Curie Grant Agreement COMPASS No. 691185. Portions of this work were inspired by a User project at the Molecular Foundry, supported by the Office of Science, Office of Basic Energy Sciences, of the U.S. Department of Energy under Contract No. DE-AC02-05CH11231.

■ REFERENCES

(1) Nozik, A. J. *Phys. E* **2002**, *14*, 115.

(2) Carey, G. H.; Abdelhady, A. L.; Ning, Z.; Thon, S. M.; Bakr, O. M.; Sargent, E. H. *Chem. Rev.* **2015**, *115* (23), 12732.

(3) Semonin, O. E.; Luther, J. M.; Choi, S.; Chen, H. Y.; Gao, J.; Nozik, A. J.; Beard, M. C. *Science* **2011**, *334* (6062), 1530.

(4) Boneschanscher, M. P.; Evers, W. H.; Geuchies, J. J.; Altantzis, T.; Goris, B.; Rabouw, F. T.; van Rossum, S. A. P.; van der Zant, H. S. J.; Siebbeles, L. D. A.; Van Tendeloo, G.; Swart, I.; Hilhorst, J.; Petukhov, A. V.; Bals, S.; Vanmaekelbergh, D. *Science* **2014**, *344* (6190), 1377.

(5) Evers, W. H.; Schins, J. M.; Aerts, M.; Kulkarni, A.; Capiod, P.; Berthe, M.; Grandidier, B.; Delerue, C.; van der Zant, H. S. J.; van Overbeek, C.; Peters, J. L.; Vanmaekelbergh, D.; Siebbeles, L. D. A. *Nat. Commun.* **2015**, *6*, 1.

(6) Kalesaki, E.; Delerue, C.; Morais Smith, C.; Beugeling, W.; Allan, G.; Vanmaekelbergh, D. *Phys. Rev. X* **2014**, *4* (1), 011010.

(7) Delerue, C. *Nat. Mater.* **2016**, *15* (5), 498.

(8) Moreels, I.; Lambert, K.; De Muynck, D.; Vanhaecke, F.; Poelman, D.; Martins, J. C.; Allan, G.; Hens, Z. *Chem. Mater.* **2007**, *19* (25), 6101.

(9) Steckel, J. S.; Yen, B. K. H.; Oertel, D. C.; Bawendi, M. G. *J. Am. Chem. Soc.* **2006**, *128* (40), 13032.

(10) Evans, C. M.; Evans, M. E.; Krauss, T. D. *J. Am. Chem. Soc.* **2010**, *132* (32), 10973.

(11) Zhang, J.; Gao, J.; Miller, E. M.; Luther, J. M.; Beard, M. C. *ACS Nano* **2014**, *8* (1), 614.

(12) Joo, J.; Pietryga, J. M.; McGuire, J. A.; Jeon, S.-H.; Williams, D. J.; Wang, H.-L.; Klimov, V. I. *J. Am. Chem. Soc.* **2009**, *131* (30), 10620.

(13) Hendricks, M. P.; Campos, M. P.; Cleveland, G. T.; Jen-La Plante, I.; Owen, J. S. *Science* **2015**, *348* (6240), 1226.

(14) Sugimoto, T. *J. Colloid Interface Sci.* **1992**, *150*, 208.

(15) Sugimoto, T.; Shiba, F.; Sekiguchi, T.; Itoh, H. *Colloids Surf., A* **2000**, *164*, 183.

(16) Owen, J. S.; Chan, E. M.; Liu, H.; Alivisatos, A. P. *J. Am. Chem. Soc.* **2010**, *132* (51), 18206.

(17) Abe, S.; Capek, R. K.; De Geyter, B.; Hens, Z. *ACS Nano* **2012**, *6* (1), 42.

(18) Koketsu, M.; Ishihara, H. In *Handbook of Chalcogen Chemistry: New Perspectives in Sulfur, Selenium and Tellurium*; Devillanova, F. A., Ed.; Royal Society of Chemistry: Cambridge, 2007; pp 145−194.

(19) Lipp, M.; Dallacker, F.; Köcker, I. Z. *Monatsh. Chem.* **1959**, *90* (1), 41.

(20) Sonoda, N.; Yamamoto, G.; Tsutsumi, S. *Bull. Chem. Soc. Jpn.* **1972**, *45*, 2937.

(21) Blum, T.; Ermert, J.; Coenen, H. H. *J. Labelled Compd. Radiopharm.* **2001**, *44* (Supplement S1), S140.

(22) Mamedov, V. A.; Zhukova, N. A.; Gubaidullin, A. T.; Beschastnova, T. N.; Rizvanov, I. K.; Levin, Y. A.; Litvinov, I. A. *Russ. Chem. Bull.* **2009**, *58* (6), 1294.

(23) Palmer, J. H.; Parkin, G. *Polyhedron* **2013**, *52* (C), 658.

(24) Zakrzewski, J.; Huras, B.; Kiełczewska, A. *Synthesis* **2015**, *48* (01), 85.

(25) Landry, V. K.; Minoura, M.; Pang, K.; Buccella, D.; Kelly, B. V.; Parkin, G. *J. Am. Chem. Soc.* **2006**, *128* (38), 12490.

(26) Anderson, N. C.; Hendricks, M. P.; Choi, J. J.; Owen, J. S. *J. Am. Chem. Soc.* **2013**, *135* (49), 18536.

(27) Murray, C. B.; Sun, S.; Gaschler, W.; Doyle, H.; Betley, T. A.; Kagan, C. R. *IBM J. Res. Dev.* **2001**, *45* (1), 47.

(28) Yu, W. W.; Falkner, J. C.; Shih, B. S.; Colvin, V. L. *Chem. Mater.* **2004**, *16* (17), 3318.

(29) Kovalenko, M. V.; Talapin, D. V.; Loi, M. A.; Cordella, F.; Hesser, G.; Bodnarchuk, M. I.; Heiss, W. *Angew. Chem., Int. Ed.* **2008**, *47* (16), 3029.

(30) Dai, Q.; Wang, Y.; Li, X.; Zhang, Y.; Pellegrino, D. J.; Zhao, M.; Zou, B.; Seo, J.; Wang, Y.; Yu, W. W. *ACS Nano* **2009**, *3* (6), 1518.

(31) Ma, W.; Swisher, S. L.; Ewers, T.; Engel, J.; Ferry, V. E.; Atwater, H. A.; Alivisatos, A. P. *ACS Nano* **2011**, *5* (10), 8140.

(32) Choi, J. J.; Lim, Y.-F.; Santiago-Berrios, M. B.; Oh, M.; Hyun, B.-R.; Sun, L.; Bartnik, A. C.; Goedhart, A.; Malliaras, G. G.; Abruña, H. D.; Wise, F. W.; Hanrath, T. *Nano Lett.* **2009**, *9* (11), 3749.

(33) Evans, C. M.; Guo, L.; Peterson, J. J.; Maccagnano-Zacher, S.; Krauss, T. D. *Nano Lett.* **2008**, *8* (9), 2896.

DOI: 10.1021/jacs.6b11021
J. Am. Chem. Soc. 2017, 139, 2296−2305

(34) Hendricks, M. P.; Cossairt, B. M.; Owen, J. S. *ACS Nano* **2012**, *6* (11), 10054.
(35) Campos, M. P.; Owen, J. S. *Chem. Mater.* **2016**, *28* (1), 227.
(36) Busby, E.; Anderson, N. C.; Owen, J. S.; Sfeir, M. Y. *J. Phys. Chem. C* **2015**, *119* (49), 27797.
(37) Peng, X.; Wickham, J.; Alivisatos, A. P. *J. Am. Chem. Soc.* **1998**, *120*, 5343.
(38) Weidman, M. C.; Beck, M. E.; Hoffman, R. S.; Prins, F.; Tisdale, W. A. *ACS Nano* **2014**, *8* (6), 6363.
(39) Cui, J.; Beyler, A. P.; Marshall, L. F.; Chen, O.; Harris, D. K.; Wanger, D. D.; Brokmann, X.; Bawendi, M. G. *Nat. Chem.* **2013**, *5* (7), 602.
(40) Cui, J.; Beyler, A. P.; Coropceanu, I.; Cleary, L.; Avila, T. R.; Chen, Y.; Cordero, J. M.; Heathcote, S. L.; Harris, D. K.; Chen, O.; Cao, J.; Bawendi, M. G. *Nano Lett.* **2016**, *16* (1), 289.
(41) Chen, O.; Zhao, J.; Chauhan, V. P.; Cui, J.; Wong, C.; Harris, D. K.; Wei, H.; Han, H.-S.; Fukumura, D.; Jain, R. K.; Bawendi, M. G. *Nat. Mater.* **2013**, *12* (1), 445.
(42) Mittleman, D.; Schoenlein, R.; Shiang, J.; Colvin, V.; Alivisatos, A.; Shank, C. *Phys. Rev. B: Condens. Matter Mater. Phys.* **1994**, *49* (20), 14435.
(43) Peterson, J. J.; Krauss, T. D. *Nano Lett.* **2006**, *6* (3), 510.
(44) Zhou, J.; Pu, C.; Jiao, T.; Hou, X.; Peng, X. *J. Am. Chem. Soc.* **2016**, *138* (20), 6475.
(45) Beecher, A. N.; Yang, X.; Palmer, J. H.; LaGrassa, A. L.; Juhas, P.; Billinge, S. J. L.; Owen, J. S. *J. Am. Chem. Soc.* **2014**, *136* (30), 10645.
(46) Norris, D. J.; Sacra, A.; Murray, C. B.; Bawendi, M. G. *Phys. Rev. Lett.* **1994**, *72* (16), 2612.
(47) Park, S. D.; Baranov, D.; Ryu, J.; Cho, B.; Halder, A.; Seifert, S.; Vajda, S.; Jonas, D. M. *Nano Lett.* **2017**, DOI: 10.1021/acs.nanolett.6b03874.
(48) Caram, J. R.; Bertram, S. N.; Utzat, H.; Hess, W. R.; Carr, J. A.; Bischof, T. S.; Beyler, A. P.; Wilson, M. W. B.; Bawendi, M. G. *Nano Lett.* **2016**, *16* (10), 6070.
(49) Grodzińska, D.; Evers, W. H.; Dorland, R.; van Rijssel, J.; van Huis, M. A.; Meijerink, A.; De Mello Donega, C.; Vanmaekelbergh, D. *Small* **2011**, *7* (24), 3493.
(50) Allan, G.; Delerue, C. *Phys. Rev. B: Condens. Matter Mater. Phys.* **2004**, *70* (24), 245321.
(51) An, J. M.; Franceschetti, A.; Zunger, A. *Nano Lett.* **2007**, *7* (7), 2129.
(52) Franceschetti, A. *Phys. Rev. B: Condens. Matter Mater. Phys.* **2008**, *78* (7), 075418.
(53) Kelley, A. M. *J. Phys. Chem. Lett.* **2010**, *1* (9), 1296.
(54) Kelley, A. M. *ACS Nano* **2011**, *5* (6), 5254.
(55) Lin, C.; Gong, K.; Kelley, D. F.; Kelley, A. M. *J. Phys. Chem. C* **2015**, *119* (13), 7491.
(56) Salvador, M. R.; Graham, M. W.; Scholes, G. D. *J. Chem. Phys.* **2006**, *125* (18), 184709.
(57) Sagar, D. M.; Cooney, R. R.; Sewall, S. L.; Dias, E. A.; Barsan, M. M.; Butler, I. S.; Kambhampati, P. *Phys. Rev. B: Condens. Matter Mater. Phys.* **2008**, *77* (23), 235321.
(58) Bullen, C. R.; Mulvaney, P. *Nano Lett.* **2004**, *4* (12), 2303.
(59) Clark, M. D.; Kumar, S. K.; Owen, J. S.; Chan, E. M. *Nano Lett.* **2011**, *11* (5), 1976.
(60) Badiello, R.; Batt, L.; Bergman, J.; Chakraborti, D.; Gsizmadia, I. G.; Engman, L.; Fringuelli, F.; Fujimori, K.; Gross, M. L.; Gysling, H. J.; Hargittai, I.; Hevesi, L.; Irgolic, K. J.; Jensen, K. A.; Kjaer, A.; Luthra, N. P.; Oae, S.; Odom, J. D.; Ogawa, A.; Okamoto, Y.; Poirier, R. A.; Renson, M.; Rozsondai, B.; Sidén, J.; Snatzke, G.; Sonoda, N.; Sturgeon, G. D.; Taticchi, A. *The Chemistry of Organic Selenium and Tellurium Compounds*; Padai, S., Rappoport, Z., Eds.; John Wiley & Sons: Chichester, UK, 1986; Vol. *1*.
(61) Hoertz, P. G.; Niskala, J. R.; Dai, P.; Black, H. T.; You, W. *J. Am. Chem. Soc.* **2008**, *130* (30), 9763.
(62) Kantlehner, W.; Hauber, M.; Vettel, M. *J. Prakt. Chem./Chem.-Ztg.* **1996**, *338*, 403.
(63) Hu, Y.; Koch, S.; Lindberg, M.; Peyghambarian, N.; Pollock, E.; Abraham, F. *Phys. Rev. Lett.* **1990**, *64* (15), 1805.
(64) Klimov, V.; Hunsche, S.; Kurz, H. *Phys. Rev. B: Condens. Matter Mater. Phys.* **1994**, *50*, 8110.

DOI: 10.1021/jacs.6b11021
J. Am. Chem. Soc. 2017, 139, 2296−2305